Bollettino di Geofisica Teorica ed Applicata Vol. 60, n. 4, pp. 549-568; December 2019
DOI 10.4430/bgta0291

Investigation of the local site effects in the northern part of the eastern Anatolian region, Turkey

E. Pamuk

Department of Geophysical Research, General Directorate of the Mineral Research & Exploration of Turkey, Ankara, Turkey

(Received: 27 December 2018; accepted: 20 June 2019)

ABSTRACT In seismically active regions, the site effect plays a very important role in planning the design of structures and estimating seismic damage to existing structures. In this study, six earthquakes ($M > 3.0$) in the northern part of the eastern Anatolian region (Turkey), recorded by 30 accelerometers located on different soil types, were investigated for local soil characteristics using horizontal-to-vertical spectral ratio (EHV) methods. The EHV results show that the predominant period values change from 0.1 to 1.2 s; also, the amplification factor (A_0) values range between 2.0 and 10.5. The soil vulnerability index (Kg) values, which are very important in hazard assessment, range from 1 to 30. The bedrock depths were calculated with the help of empirical relations between the soil predominant period and soft soil thickness. The bedrock depths change from 0 to 110 m. Soil characterisation based on S-wave velocity (V_S) is one of the main factors for estimating seismic damages. V_S was evaluated using previous results from the surface waves method at 11 accelerometer stations. V_{S30} values are observed within the range of 250-750 m/s. For detailed study, five accelerometer stations were selected and V_S-depth cross-sections, borehole results, and SPT-N values were used.

Key words: earthquake, EHV, predominant period, bedrock, vulnerability index.

1. Introduction

In Turkey, there are several major fault systems located in the Alpine-Himalayan orogenic belt, such as the East Anatolian Fault zone (EAFZ), the North Anatolian Fault Zone (NAFZ), The NAFZ is one of the world's largest strike-slip fault zones and this zone consists of a cross-continental plate (Tatar *et al*., 2013). This fault zone extends to the Saroz bay in the north of the Aegean Sea and has an approximate length of 1200 km (Şengör *et al*., 2005). In this fault zone, the following destructive earthquakes occurred, from east to west (Fig. 1): the 1939 Erzincan, 1942 Erbaa-Niksar, 1943 Tosya, 1944 Bolu-Gerede, 1957 Abant, 1967 Mudurnu Valley, and 1999 Kocaeli earthquakes. The largest of these earthquakes is the 1939 Erzincan earthquake (M = 7.9-8.0) (Tatar *et al*., 2013).

Depending on tectonic and geologic characteristics, the northern part of the study area, located in the NE of Turkey, generally shows an irregular terrain morphology because of the steep slopes and peaks due to the geology. The eastern Pontide Orogenic Belt, which forms a mountain chain of approximately 100 km wide and 500 km long along the south-eastern coast of the Black Sea,

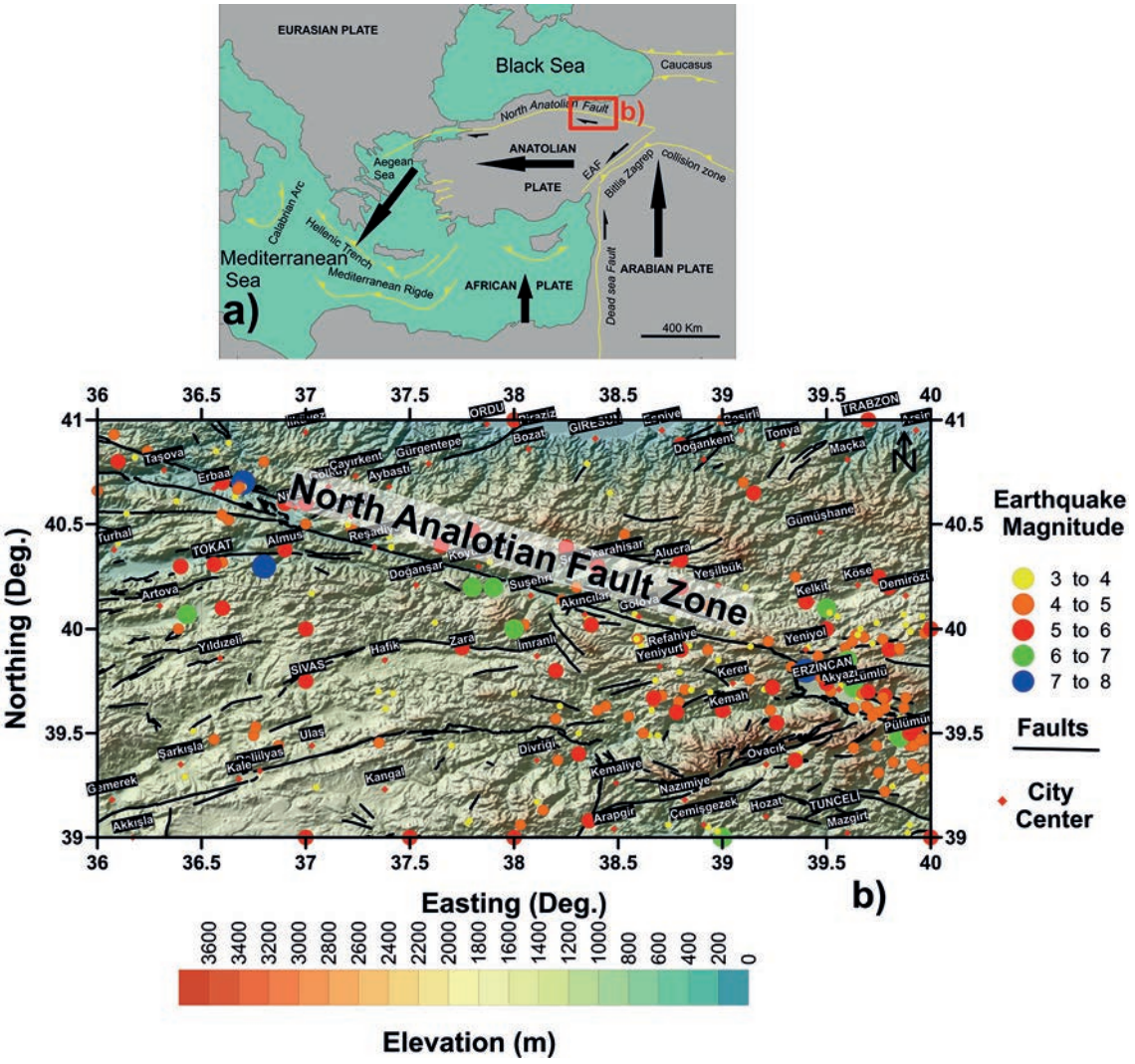

Fig. 1 - The study area together with a) tectonic setting of Anatolian plate; b) general morphology, tectonic and seismicity.

is an important metallogenetic area on the eastern coast of the Black Sea. According to Arslan *et al*. (1997), the north-eastern Pontides, which is tectonically a paleo-island arc, has experienced extensive volcanic activity from the Liassic to the Tertiary. The eastern Pontides is divided into the northern and eastern parts according to structural and lithological differences (Gedikoğlu *et al*., 1979; Bektaş *et al*., 1995). At the time that the eastern region was dominated by the Late Cretaceous and Middle Eocene volcanic and volcaniclastic rocks, the Late Cretaceous-aged sedimentary rocks became widely apparent in the southern region (Babacan and Akın, 2018). The Erzincan Basin in the south-eastern part of the study area is covered with unconsolidated Plio-Quaternary sediments. These sediments contain playa deposits, clastics, and basin margin conglomerates. The conglomerates are composed of ophiolite melange rocks and carbonates. Silt, sand, and gravels are observed mostly in the centre of the basin (Barka and Gülen, 1989). The Sivas Basin in the SW of the study area occurred on the basis of pre-Maastrichtian platform carbonates

and metamorphic-ophiolitic rocks. The Maastrichtian-Paleocene aged limestones unconformably overlie the basement in the Sivas Basin. This unit moves upwards inside the Palaeocene basaltic lavas and Eocene clastic rocks. Lower Miocene cryogenic rocks (carbonates) can be seen on the old units. Plio-Quaternary fluvial deposits and Quaternary alluvium units overlie the clastic rocks unconformably (Yilmaz and Yilmaz, 2006). The Niksar, Taşova-Erbaa Basins, in the western part of the study area, were formed along the eastern half of the North Anatolian Fault. The Taşova-Erbaa Basin is about 65 km long and 15-18 km wide. The Paleozoic metamorphics, which are the main units around the basin, are Mesozoic and Eocene volcanics (Barka *et al*., 2000). The geological map of the study area is shown in Fig. 2.

In the first step of this study, site effects were studied at 30 accelerometer stations within the study area by using horizontal-to-vertical spectral ratios (EHVs) (Langston, 1977). The EHV method was utilised for six earthquakes with the aim of investigating site effects between the 0.5-10.0 Hz frequency band for each station. In so doing, predominant periods of soil and amplitude of EHV spectra were determined. In the second stage, the seismic vulnerability index (*Kg*) was calculated with the help of empirical relations between soil predominant period and amplification factor in EHV spectra. *Kg* was used to determine the earthquake damage and the *Kg* provided information about local site effect with the help of earthquake data. Based upon this

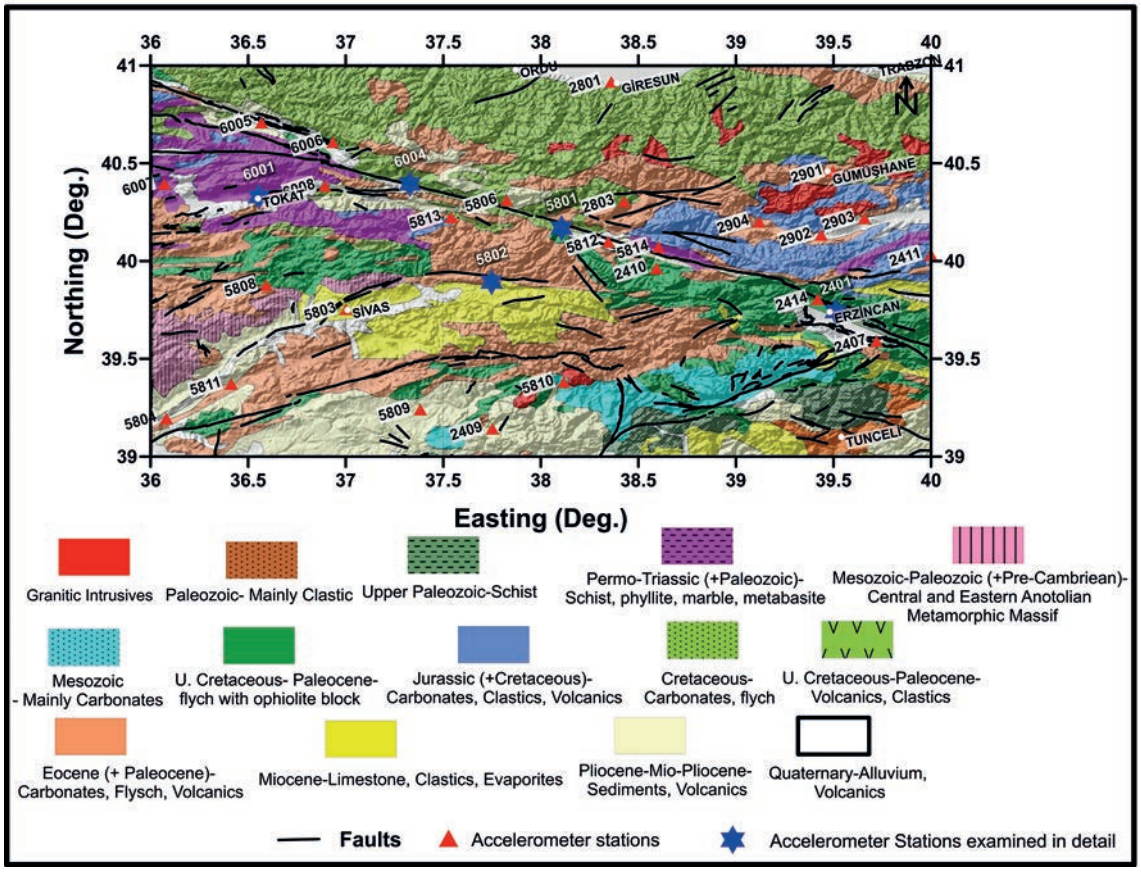

Fig. 2 - Representation of the geological map of the study area together with geomorphology and tectonic [geological map simplified from MTA (2002), active faults from Emre *et al*. (2013)].

research, horizontal deformation changes could occur at elastoplastic or plastic limits under the effect of dynamic loads where *Kg* values are higher than 20. The possible occurrence of elastic deformation is high in areas where *Kg* values are lower than 20. In the next stage, the bedrock depths were calculated through empirical relations between soil predominant period and soft soil thickness. Bedrock depth is a very important parameter in seismic risk analysis and local site effect studies, because the effects of earthquake waves on the surface are influenced by local site conditions (seismic impedances and sediment thickness overlying the bedrock). In the last step of the study, the results of previous geotechnical studies, i.e. (V_S-depth cross sections, standard penetration test (SPT-N), groundwater level (GWL), and borehole studies, carried out in the frame of the TÜBİTAK Research Project No. 105G016, were examined.

2. Data and methods

The EHV of earthquakes gives information about local site effects while removing the source and path effects (Langston, 1977). This method generally assumes that there will not be an extreme change in the amplitude of vertical component waves, and contrary horizontal component waves will be affected by the soil properties through which it passes. Vertical components cannot be amplified around the frequency range where the horizontal component receives large amplification (Nakamura, 2000). The EHV method proposed by Langston (1977) was used to obtain the crust and upper mantle structures using teleseismic data. The EHV method, which does not require a reference station, assumes that the vertical component of motion is not influenced by the local structure, whereas the horizontal components contain the P-to-S conversions due to local geological layering. Therefore, the soil response can be obtained by dividing the horizontal component amplitude spectra by the vertical component amplitude spectra. The technique has been applied in many studies (e.g. Lermo and Chavez-Garcia, 1993; Lachet *et al*., 1996; Bonilla *et al*., 1997; Parolai and Richwalski, 2004; Yalcinkaya and Alptekin, 2005a, 2005b; Parolai, 2012; Ozer, 2016, 2019).

Acceleration records in the frequency media were examined using the Fourier spectrum. Several earthquakes occurring from 2008 to 2018 recorded by 30 accelerometer stations under the control of AFAD (Prime Ministry Disaster and Emergency Management Authority in Turkey) were selected. Fig. 2 shows the locations of these stations.

The magnitudes of the earthquakes recorded from 2008 to 2018 vary between 3.0 and 5.8. Six earthquake records were used for each station. These stations consisted of Guralp CMG-5TD, Sara acebox, and GeoSig gmsplus accelerometers. Data from the stations operated by AFAD were digitised at 0.01-s intervals. Window length was selected as each earthquake duration to obtain local soil effects. Then, the amplitude spectra of three components of the earthquake data were smoothed with Konno and Ohmachi (1998) filters to remove small oscillations (noise). Table 1 provides detailed information about the earthquakes.

For data in the window, the amplitude spectra of the three components were computed using a fast Fourier transform (FFT) algorithm. EHV spectra were obtained from the ratio of the average spectra of the horizontal component to the vertical components (Fig. 3). Predominant period values were determined using the EHV spectra.

Table 1 - The earthquakes recorded by stations between June 2008 and September 2018.

Station Code	Earthquake number	Epicentre Coordinates	Earthquake Depth (km)	Earthquake Magnitude	Earthquake Date
2407	EQ1	37.58360N-38.50360E	9.79	5.1 (Mw)	2018/04/24
	EQ2	40.26760N-40.91810E	12.39	3.0 (Ml)	2018/04/22
	EQ3	39.92510N-40.72560E	11.87	3.1 (Ml)	2017/07/16
	EQ4	40.05660N-40.70500E	6.41	4.7 (Mw)	2017/05/11
	EQ5	40.06150N-40.72810E	16.35	3.9 (Mw)	2017/05/11
	EQ6	39.57980N-39.72000E	3.19	4.5 (Mw)	2016/12/16
2409	EQ1	39.13300N-37.75180E	0.10	3.0 (Ml)	2018/06/11
	EQ2	38.70300N-38.08430E	11.48	3.7 (Mw)	2018/06/18
	EQ3	38.70580N-38.08430E	7.02	3.4 (Ml)	2018/06/21
	EQ4	38.76610N-37.95250E	7.0	3.7 (Mw)	2018/07/21
	EQ5	37.37730N-36.38550E	10.53	4.8 (Mw)	2018/08/19
	EQ6	38.29110N-38.81050E	6.97	3.3 (Ml)	2018/09/03
2410	EQ1	39.95260N-38.59260E	6.36	4.0 (Mw)	2016/11/20
	EQ2	39.57980N-39.72000E	3.19	4.5 (Mw)	2016/12/16
	EQ3	39.86510N-39.60410E	7.01	3.0 (Ml)	2017/04/01
	EQ4	39.76610N-39.47460E	8.46	4.1 (Mw)	2017/05/20
	EQ5	39.93810N-39.62280E	12.10	4.0 (Mw)	2017/08/10
	EQ6	37.58360N-38.50360E	9.79	5.1 (Mw)	2018/04/24
2411	EQ1	40.02150N-39.99900E	1.76	3.2 (Ml)	2018/03/31
	EQ2	40.01330N-40.00950E	7.0	3.0 (Ml)	2018/04/03
	EQ3	37.58360N-38.50360E	9.79	5.1 (Mw)	2018/04/24
	EQ4	40.05950N-39.55260E	7.42	3.5 (Mw)	2018/04/26
	EQ5	39.95310N-40.03710E	7.02	3.8 (Mw)	2018/05/02
	EQ6	40.07850N-39.51300E	6.98	3.3 (Mw)	2018/07/23
2414	EQ1	39.26800N-40.22400E	10.8	4.1 (Mw)	2018/03/07
	EQ2	38.49450N-39.12450E	6.96	3.8 (Mw)	2018/03/30
	EQ3	40.02150N-39.99900E	1.76	3.2 (Ml)	2018/03/31
	EQ4	39.00600N-39.86950E	7.02	3.1 (Ml)	2018/04/19
	EQ5	40.05950N-39.55260E	7.42	3.5 (Mw)	2018/04/26
	EQ6	40.07850N-39.51300E	6.98	3.3 (Mw)	2018/07/23
2801	EQ1	39.57980N-39.72000E	3.19	4.5 (Mw)	2016/12/16
	EQ2	40.05660N-40.70500E	6.41	4.7 (Mw)	2017/05/11
	EQ3	40.76210N-38.52360E	7.08	3.2 (Ml)	2017/05/12
	EQ4	39.76610N-39.47460E	8.46	4.1 (Mw)	2017/05/20
	EQ5	39.99810N-40.04600	8.37	4.2 (Mw)	2018/03/03
	EQ6	40.05950N-39.55260E	7.42	3.5 (Mw)	2018/04/26

Table 1 - continued.

Station Code	Earthquake number	Epicentre Coordinates	Earthquake Depth (km)	Earthquake Magnitude	Earthquake Date
2803	EQ1	39.95160N-38.58830E	10.55	3.8 (Mw)	2016/11/21
	EQ2	39.57980N-39.72000E	3.19	4.5 (Mw)	2016/12/16
	EQ3	40.76210N-38.52360E	7.08	3.2 (Ml)	2017/05/12
	EQ4	39.99810N-40.04600	8.37	4.2 (Mw)	2018/03/03
	EQ5	40.05950N-39.55260E	7.42	3.5 (Mw)	2018/04/26
	EQ6	40.07850N-39.51300E	6.98	3.3 (Mw)	2018/07/23
2901	EQ1	39.93810N-39.62280E	12.10	4.0 (Mw)	2017/08/10
	EQ2	39.99810N-40.04600	8.37	4.2 (Mw)	2018/03/03
	EQ3	40.05950N-39.55260E	7.42	3.5 (Mw)	2018/04/26
	EQ4	39.95310N-40.03710E	7.02	3.8 (Mw)	2018/05/02
	EQ5	40.07850N-39.51300E	6.98	3.3 (Mw)	2018/07/23
	EQ6	40.88500N-40.08710E	7.22	3.0 (Ml)	2018/08/21
2902	EQ1	40.05500N-39.66400E	7.42	3.0 (Ml)	2017/11/07
	EQ2	39.99810N-40.04600E	8.37	4.2 (Mw)	2018/03/03
	EQ3	39.08850N-40.27950E	7.00	4.2 (Mw)	2018/03/07
	EQ4	37.58360N-38.50360E	9.79	5.1 (Mw)	2018/04/24
	EQ5	40.05950N-39.55260E	7.42	3.5 (Mw)	2018/04/26
	EQ6	40.07850N-39.51300E	6.98	3.3 (Mw)	2018/07/23
2903	EQ1	40.01330N-40.00950E	7.0	3.0 (Ml)	2018/04/03
	EQ2	37.58360N-38.50360E	9.79	5.1 (Mw)	2018/04/24
	EQ3	40.05950N-39.55260E	7.42	3.5 (Mw)	2018/04/26
	EQ4	39.95310N-40.03710E	7.02	3.8 (Mw)	2018/05/02
	EQ5	40.07850N-39.51300E	6.98	3.3 (Mw)	2018/07/23
	EQ6	40.88500N-40.08710E	7.22	3.0 (Ml)	2018/08/21
2904	EQ1	39.81050N-39.02630E	18.95	3.6 (Mw)	2017/10/21
	EQ2	39.99810N-40.04600E	8.37	4.2 (Mw)	2018/03/03
	EQ3	40.02150N-39.99900E	1.76	3.2 (Ml)	2018/03/31
	EQ4	37.58360N-38.50360E	9.79	5.1 (Mw)	2018/04/24
	EQ5	40.05950N-39.55260E	7.42	3.5 (Mw)	2018/04/26
	EQ6	40.07850N-39.51300E	6.98	3.3 (Mw)	2018/07/23
5803	EQ1	40.67780N-36.68200E	20.53	4.9 (Mw)	2015/10/09
	EQ2	38.81730N-37.84930E	17.54	4.5 (Mw)	2015/12/09
	EQ3	39.56400N-34.35800E	13.60	5.0 (Mw)	2016/01/10
	EQ4	39.95260N-38.59260E	6.36	4.0 (Mw)	2016/11/20
	EQ5	40.17000N-37.02810E	6.99	3.8 (Mw)	2017/05/11
	EQ6	37.58360N-38.50360E	9.79	5.1 (Mw)	2018/04/24

Table 1 - continued.

Station Code	Earthquake number	Epicentre Coordinates	Earthquake Depth (km)	Earthquake Magnitude	Earthquake Date
5804	EQ1	39.95260N-38.59260E	6.36	4.0 (Mw)	2016/11/20
	EQ2	39.65550N-35.50300E	6.06	3.7 (Mw)	2017/01/08
	EQ3	37.59550N-38.48660E	9.76	5.5 (Mw)	2017/03/02
	EQ4	39.06960N-35.92280E	21.99	3.5 (Mw)	2017/07/04
	EQ5	37.58360N-38.50360E	9.79	5.1 (Mw)	2018/04/24
	EQ6	38.35330N-36.21500E	10.44	3.9 (Mw)	2018/07/18
5806	EQ1	39.95260N-38.59260E	6.36	4.0 (Mw)	2016/11/20
	EQ2	39.57980N-39.72000E	3.19	4.5 (Mw)	2016/12/16
	EQ3	39.61700N-37.38350E	3.76	3.2 (Mw)	2017/01/09
	EQ4	40.76210N-38.52360E	7.08	3.2 (Mw)	2017/05/12
	EQ5	37.58360N-38.50360E	9.79	5.1 (Mw)	2018/04/24
	EQ6	40.05950N-39.55260E	7.42	3.5 (Mw)	2018/04/26
5808	EQ1	40.67780N-36.68200E	20.53	4.9 (Mw)	2015/10/09
	EQ2	38.84010N-37.83700E	22.41	5.0 (Mw)	2015/11/29
	EQ3	39.56400N-34.35800E	13.60	5.0 (Mw)	2016/01/10
	EQ4	39.95260N-38.59260E	6.36	4.0 (Mw)	2016/11/20
	EQ5	40.17000N-37.02810E	6.99	3.8 (Mw)	2017/05/11
	EQ6	37.58360N-38.50360E	9.79	5.1 (Mw)	2018/04/24
5809	EQ1	38.28680N-37.18160E	12.00	4.0 (Mw)	2017/03/28
	EQ2	39.24580N-38.13660E	5.04	3.0 (Ml)	2018/01/11
	EQ3	39.13300N-37.75180E	0.10	3.0 (Ml)	2018/06/11
	EQ4	38.70300N-38.08430E	11.48	3.7 (Mw)	2018/06/18
	EQ5	38.70580N-38.08430E	7.02	3.4 (Ml)	2018/06/21
	EQ6	38.76610N-37.95250E	7.0	3.4 (Mw)	2018/07/21
5810	EQ1	38.49450N-39.12450E	6.96	3.8 (Mw)	2018/03/30
	EQ2	37.58360N-38.50360E	9.79	5.1 (Mw)	2018/04/24
	EQ3	39.13300N-37.75180E	0.10	3.0 (Ml)	2018/06/11
	EQ4	38.70300N-38.08430E	11.48	3.7 (Mw)	2018/06/18
	EQ5	38.70580N-38.08430E	7.02	3.4 (Ml)	2018/06/21
	EQ6	38.76610N-37.95250E	7.0	3.4 (Mw)	2018/07/21
5811	EQ1	39.69780N-37.73780E	21.25	3.0 (Ml)	2016/10/26
	EQ2	39.65550N-35.50300E	6.06	3.7 (Mw)	2017/01/08
	EQ3	37.59550N-38.48660E	9.76	5.5 (Mw)	2017/03/02
	EQ4	38.28680N-37.18160E	12.00	4.0 (Mw)	2017/03/28
	EQ5	39.06960N-35.92280E	21.99	3.5 (Mw)	2017/07/04
	EQ6	37.58360N-38.50360E	9.79	5.1 (Mw)	2018/04/24

Table 1 - continued.

Station Code	Earthquake number	Epicentre Coordinates	Earthquake Depth (km)	Earthquake Magnitude	Earthquake Date
5812	EQ1	37.59550N-38.48660E	9.76	5.5 (Mw)	2017/03/02
	EQ2	39.73730N-38.84810E	5.01	3.1 (Mw)	2017/04/27
	EQ3	39.67480N-38.82130E	6.99	3.1 (Ml)	2017/06/28
	EQ4	39.99810N-40.04600E	8.37	4.2 (Mw)	2018/03/03
	EQ5	37.58360N-38.50360E	9.79	5.1 (Mw)	2018/04/24
	EQ6	40.05950N-39.55260E	7.42	3.5 (Mw)	2018/04/26
5813	EQ1	39.95260N-38.59260E	6.36	4.0 (Mw)	2016/11/20
	EQ2	39.57980N-39.72000E	3.19	4.5 (Mw)	2016/12/16
	EQ3	39.65550N-35.50300E	6.06	3.7 (Mw)	2017/01/08
	EQ4	40.17000N-37.02810E	6.99	3.8 (Mw)	2017/05/11
	EQ5	37.58360N-38.50360E	9.79	5.1 (Mw)	2018/04/24
	EQ6	40.70250N-35.48030E	7.12	4.1 (Mw)	2018/05/18
5814	EQ1	39.93810N-39.62280E	12.10	4.0 (Mw)	2017/08/10
	EQ2	39.81050N-39.02630E	18.95	3.6 (Mw)	2017/10/21
	EQ3	39.99810N-40.04600E	8.37	4.2 (Mw)	2018/03/03
	EQ4	37.58360N-38.50360E	9.79	5.1 (Mw)	2018/04/24
	EQ5	40.05950N-39.55260E	7.42	3.5 (Mw)	2018/04/26
	EQ6	40.07850N-39.51300E	6.98	3.3 (Mw)	2018/07/23
6005	EQ1	40.55850N-36.72210E	17.52	3.0 (Ml)	2017/04/24
	EQ2	40.17000N-37.02810E	6.99	3.8 (Mw)	2017/05/11
	EQ3	40.54460N-36.59750E	15.8	4.0 (Mw)	2018/01/06
	EQ4	40.55280N-36.57850E	7.49	3.4 (Ml)	2018/01/06
	EQ5	40.67410N-35.48910E	10.02	3.7 (Mw)	2018/03/29
	EQ6	37.58360N-38.50360E	9.79	5.1 (Mw)	2018/04/24
6006	EQ1	40.49800N-37.20180E	11’0	3.6 (Mw)	2016/11/08
	EQ2	40.17000N-37.02810E	6.99	3.8 (Mw)	2017/05/11
	EQ3	40.54460N-36.59750E	15.8	4.0 (Mw)	2018/01/06
	EQ4	40.55280N-36.57850E	7.49	3.4 (Ml)	2018/01/06
	EQ5	37.58360N-38.50360E	9.79	5.1 (Mw)	2018/04/24
	EQ6	40.70250N-35.48030E	7.12	4.1 (Mw)	2018/05/18
6007	EQ1	38.84010N-37.83700E	22.41	5.0 (Mw)	2015/11/29
	EQ2	39.56400N-34.35800E	13.60	5.0 (Mw)	2016/01/10
	EQ3	40.54100N-35.76930E	9.92	3.0 (Ml)	2016/02/21
	EQ4	40.54460N-36.59750E	15.8	4.0 (Mw)	2018/01/06
	EQ5	40.55960N-35.79010E	14.3	3.6 (Mw)	2018/01/19
	EQ6	40.22910N-35.62100E	16.85	3.2 (Ml)	2018/06/25

Table 1 - continued.

Station Code	Earthquake number	Epicentre Coordinates	Earthquake Depth (km)	Earthquake Magnitude	Earthquake Date
6008	EQ1	40.54460N-36.59750E	15.8	4.0 (Mw)	2018/01/06
	EQ2	40.55280N-36.57850E	7.49	3.4 (Ml)	2018/01/06
	EQ3	40.55960N-35.79010E	14.3	3.6 (Mw)	2018/01/19
	EQ4	37.58360N-38.50360E	9.79	5.1 (Mw)	2018/04/24
	EQ5	40.70250N-35.48030E	7.12	4.1 (Mw)	2018/05/18
	EQ6	40.22910N-35.62100E	16.85	3.2 (Ml)	2018/06/25

3. Predominant period and amplification factor

Fig. 3 presents the EHV graphs obtained for stations located on different soil types in the study area. The obtained EHV spectra for all earthquakes are shown in a single graph by station. A single representative EHV curve for each station was obtained by calculating the geometric means of the EHV spectra. There are nine stations (2401, 2414, 2801, 2903, 6001, 6004, 6005, 6006, and 6007) on alluvium units known to be a weak zone in the study area. The predominant period values are 0.38 and 0.54 s and the amplification factors are 2.86 and 2.81 in stations 2401 and 2414 in the Erzincan Basin, respectively. In stations 6001, 6004, 6005, and 6006 in the northern part of Tokat city, the predominant period values are 0.51, 1.25, 0.22, and 0.77 s, while the amplification factors are 10.70, 2.69, 4.63, and 3.42, respectively. In station 2903, located in the southern part of Giresun city, the predominant period value is 0.53 s and the amplification factor is 3.53. In station 6007, located in the western part of Tokat, the predominant period is 0.84 s and the amplification factor is 4.36. In station 2801 in the southern part of Giresun, the predominant period value is 1.33 s and the amplification factor is 2.42. In stations 2409, 5809, 6008, and 5801 on Pliocene, Mio-Pliocene sediments, and volcanics, the predominant period values are 0.30, 0.26, 0.82, and 0.32 s and the amplification factors are 3.04, 5.25, 4.40, and 2.26, respectively. In stations 5802 and 5803 on Miocene limestones, clastics, and evaporites, the predominant period values are 0.27 and 0.13 s and the amplification factors are 5.29 and 2.00, respectively. In stations 2901, 2902, 2904, 5808, 5811, and 5812 on Eocene carbonate, flysch, and volcanics, the predominant period values are 0.19, 0.18, 0.60, 0.11, 0.45, and 0.38 s and the amplification factors are 5.33, 2.60, 2.59, 1.95, 6.52, and 3.00, respectively. In stations 5806, 2803, and 5813 on Cretaceous carbonate and flysch, the predominant period values are 0.19, 0.49, and 1.20 s and the amplification factors are 3.41, 3.01, and 2.20, respectively. In station 2411 on Jurassic carbonate, clastic, and volcanics, the predominant period value is 0.28 s and the amplification factor is 6.91. In stations 2410 and 2407 on Cretaceous and Paleocene ophiolitic rocks, the predominant period values are 0.10 and 0.35 s; the amplification factors are 2.72 and 2.65, respectively. In station 5810 on Mesozoic carbonates, the predominant period value is 0.11 s; the amplification factor is 4.81.

The frequency value corresponding to the highest amplitude from EHV spectral ratio graphs was determined and converted to the period unit. The obtained soil-predominant period values were mapped (Fig. 4). The predominant period values in the study area range from 0.10 to 1.20 s. Maximum period values were obtained in the east part of Tokat and around Giresun. The

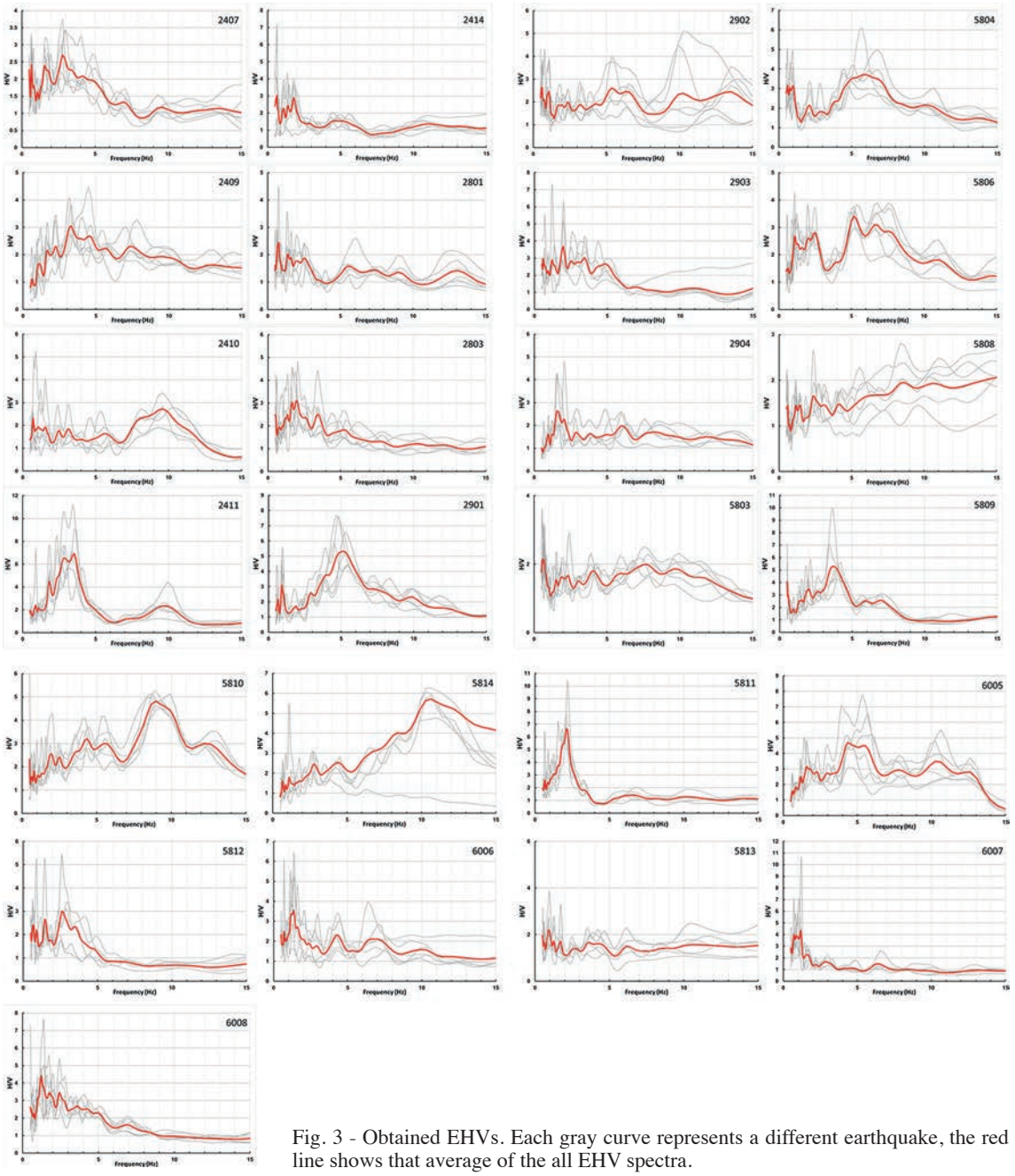

Fig. 3 - Obtained EHVs. Each gray curve represents a different earthquake, the red line shows that average of the all EHV spectra.

lower predominant period values were observed in the south and SW parts of the study area. The period values in the Erzincan Basin are approximately 0.5 s. There is a noteworthy increase in the period values from the south to the north of the study area. In addition, V_{S30} (the average S-wave velocity of the uppermost 30 m of a soil column) values were seen in 11 of 30 stations. V_{s30} values at these eleven stations were obtained from previous studies by AFAD. There is no information about V_{s30} values at the other stations. These stations are: 5804, 5803, 6001, 6005, 6004, 5801, 5802, 2901, 2902, 2401, and 2407. The distribution of the V_{S30} values at these stations is also

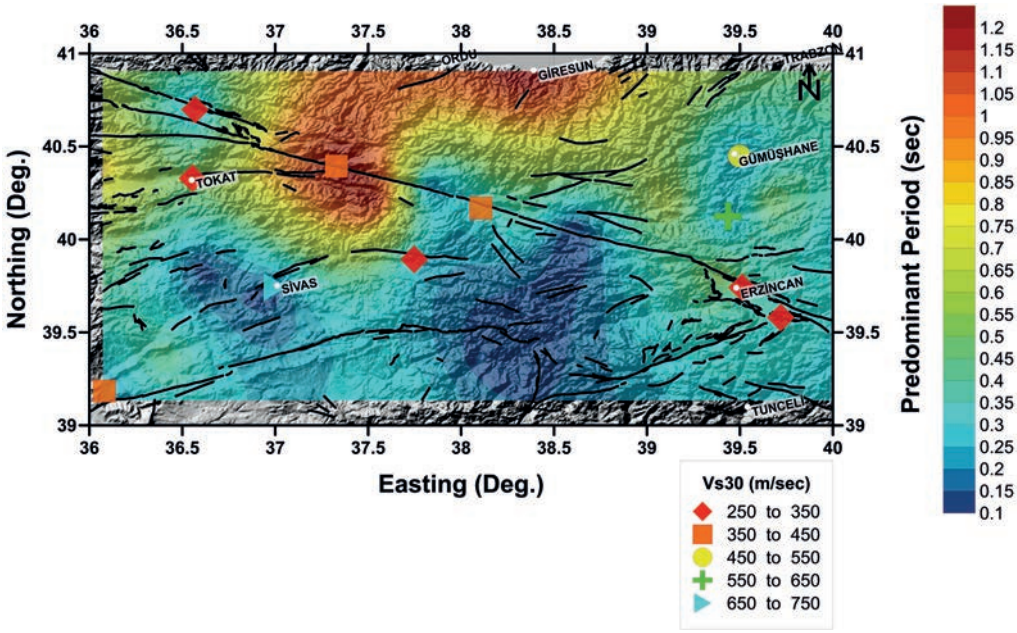

Fig. 4 - Predominant period distribution map overlaid on the shaded relief topographic map of the study area with the V_{S30} values.

shown on the predominant period map (Fig. 4). In the area where the period value is above 1.0 s in the eastern part of Tokat, V_{S30} values range between 350-450 m/s. Although the V_{s30} values range between 650-750 m/s in this part, the period values around Sivas city range between 0.1 and 0.2 s. These values are 250-350 m/s in the Erzincan Basin. V_S values range between 450-550 m/s in this part; however, the period values around Gümüşhane city are approximately 0.3-0.4 s. The V_{S30} values in Tokat and in the north part of this city range between 250-350 m/s. The period values in these regions range between 0.4-0.7 s.

The maximum amplitude values of the EHV graphs were determined and mapped (Fig. 5). The amplification values in the study area vary between 2 and 11. The maximum amplification values were obtained around Tokat. Lower amplification values were observed in the northern and the south-eastern parts of the study area. The amplification values in the Erzincan Basin are around 3. There is a noteworthy increase in the period values from the south to the north of the study area. The amplification values around Sivas range between 2.0 and 2.5 (Fig. 5).

4. Vulnerability index (*Kg*)

Nakamura (1997, 2000) argued that there are relations between *Kg* values that are calculated from maximum amplitude-frequency values in EHV spectra. With the help of this technique, the soil weak regions in the study area can be determined and the areas where damage might occur before an earthquake can be estimated using Eq. 1:

$$Kg = A^2/F \quad (1)$$

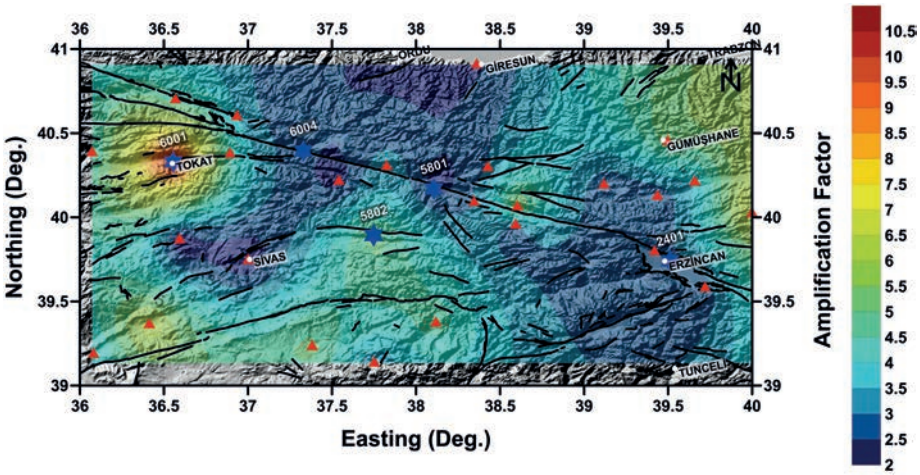

Fig. 5 - EHV amplitude distribution map overlaid on the shaded relief topographic map of the study area with the accelometer stations.

where *Kg* is the vulnerability index, *A* is the amplification factor, and *F* is the predominant frequency. The *Kg* value is used for determining soil weak regions and calculating the possibility of damage (Beroya *et al*., 2009; Warnana *et al*., 2011; Kyaw *et al*., 2014; Adib *et al*., 2015; Sugianto *et al*., 2016; Pamuk *et al*., 2018). In the evaluation of the *Kg* distribution map (Fig. 6), *Kg* values range between 1 and 30. Maximum *Kg* values were obtained in Tokat and its surroundings and the south-western part of Sivas. *Kg* values, especially around Tokat, are greater than 20. This value is between 10 and 15 in the east of Gümüşhane and this value is lower than 10 in Sivas. The map of *Kg* is generally compatible with the amplification factor and predominant period map. In areas where the amplification values are high, high *Kg* values were obtained and in areas where the amplification values were low, low *Kg* values were obtained (Figs. 5 and 6). In the eastern part of Tokat, the predominant period values are high ($t_0 > 0.7$ s) and the *Kg* values range from 10 to 20. In the eastern part of Tokat, the predominant period values are high ($t_0 > 0.7$ s); high *Kg* values were obtained from 10 to 20.

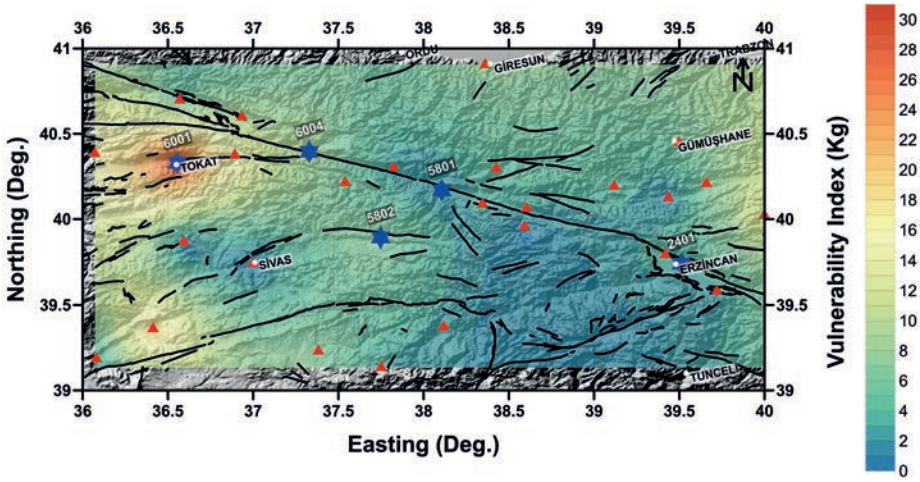

Fig. 6 - *Kg* distribution map overlaid on the shaded relief topographic map of the study area with the accelometer stations.

5. Bedrock depth estimation

Bedrock depth and the geometry of the bedrock surface are important parameters for engineering seismological studies. When seismic studies are not available, and hence V_S-depth profiles cannot be obtained, correlation techniques can be used to accurately obtain bedrock depth. The EHV method can be used to rapidly estimate the depth to bedrock. Regression equations can be used to estimate bedrock depth.

In this study, five different formulae were used for the depth of bedrock with the help of the relation between soft soil thickness and the soil predominant period (Table 2) (Ibs-von Seth and Wohlenberg, 1999; Delgado *et al*., 2000; Parolai *et al*., 2002; Dinesh *et al*., 2010; Molnar *et al*., 2018).

The bedrock depths obtained using five different formulae were averaged. Thus, bedrock depths were obtained for the study area, as shown in Fig. 7. Bedrock depth varies between 0 and 110 m in the study area. The deepest bedrock depth was obtained in the northern parts of the study area. In the southern and south-western parts of the study area, bedrock depth ranges between 0-20 m. The period values in the Erzincan Basin are around 0.5 s. There is a noteworthy increase in the period values from the south to the north of the study area (Fig. 7).

6. V_S-depth cross sections, SPT-N values, and borehole studies in stations 2401, 5801, 5802, 6001, and 6004

Five accelerometer stations (2401, 5801, 5802, 6001, and 6004) operated by AFAD were selected for a detailed study. Table 3 gives the parameters used in these stations related to the earthquakes. For detailed study, V_S-depth cross-sections, borehole results, and SPT-N values from the Report on Seismic and Geotechnical Investigations from the TÜBİTAK Research Project, No. 105G016, were used (Fig. 8).

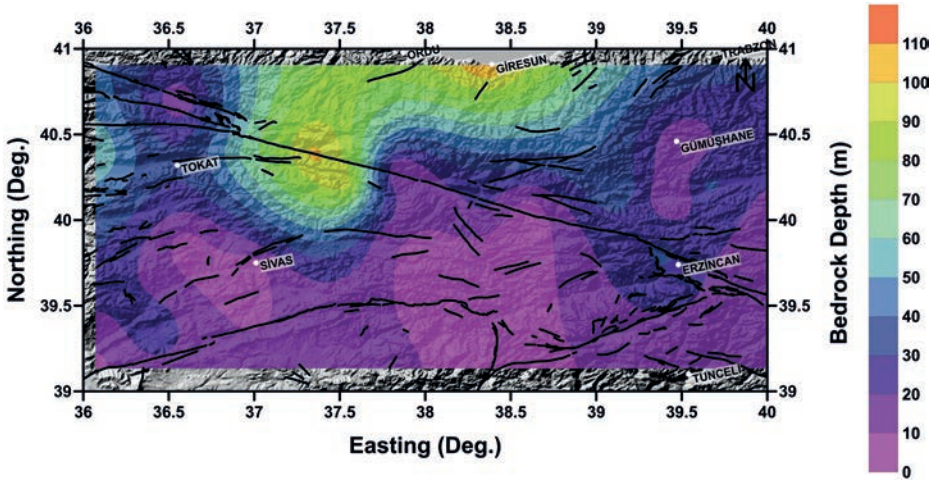

Fig. 7 - Bedrock depth distribution map overlaid on the shaded relief topographic map of the study area with the accelometer stations.

Table 2 - Obtained bedrock depth values for all stations using five different formulae (d = depth of the bedrock; f = predominant frequency).

Station Code	Molnar *et al.* (2018) $d=64.98*(f^{-1.198})$	Delgado *et al.* (2000) $d=55.64*(f^{-1.268})$	Dinesh *et al.* (2009) $d=58.30*(f^{-0.952})$	Parolai *et al.* (2002) $d=108*(f^{-1.551})$	Ibs-von Seht and Wohlenberg (1999) $d=96*(f^{-1.388})$	Average Bedrock Depth (m)
2407	18.3	14.6	21.3	20.9	22.1	19.4
2409	15.5	12.2	18.7	17.0	18.3	16.4
2410	4.3	3.2	6.8	3.2	4.2	4.3
2411	14.3	11.2	17.5	15.2	16.6	15.0
2414	31.3	25.7	32.6	41.9	41.2	34.5
2801	91.7	80.1	76.7	168.7	143.1	112.1
2803	27.7	22.5	29.6	35.7	35.7	30.2
2901	9.1	6.9	12.2	8.4	9.8	9.3
2902	8.7	6.6	11.8	8.0	9.4	8.9
2903	30.1	24.7	31.6	39.9	39.4	33.1
2904	35.4	29.3	36.0	49.2	47.5	39.5
5803	5.8	4.3	8.5	4.7	5.8	5.8
5804	7.7	5.8	10.7	6.8	8.1	7.8
5806	9.1	6.9	12.2	8.4	9.8	9.3
5808	4.9	3.6	7.5	3.8	4.8	4.9
5809	13.2	10.3	16.4	13.7	15.1	13.7
5810	4.7	3.5	7.2	3.6	4.6	4.7
5811	25.4	20.6	27.6	32.0	32.3	27.6
5812	20.7	16.6	23.5	24.5	25.5	22.1
5813	81.2	70.5	69.6	144.2	124.3	98.0
5814	3.8	2.8	6.2	2.8	3.6	3.8
6005	10.7	8.3	13.9	10.5	11.9	11.1
6006	47.5	39.9	45.4	71.9	66.7	54.3
6007	53.3	45.1	49.8	83.5	76.3	61.6
6008	51.2	43.2	48.2	79.3	72.8	59.0
2401	19.9	15.9	22.7	23.3	24.3	21.2
5801	16.9	13.4	20.0	18.9	20.1	17.8
5802	13.7	10.7	17.0	14.4	15.9	14.3
6001	28.8	23.6	30.6	37.7	37.5	31.6
6004	84.9	73.8	72.1	152.7	130.9	102.9

Examining station 2401, located on Quaternary alluvium in the Erzincan Basin, it is revealed that the V_S values range between 200 and 470 m/s from the surface to a depth of 30 m. The SPT-N values range from 4 to 44. It can be seen that the SPT-N values, which generally increase with the depth, are consistent with the V_S values. The underground water level is located at 10 m below

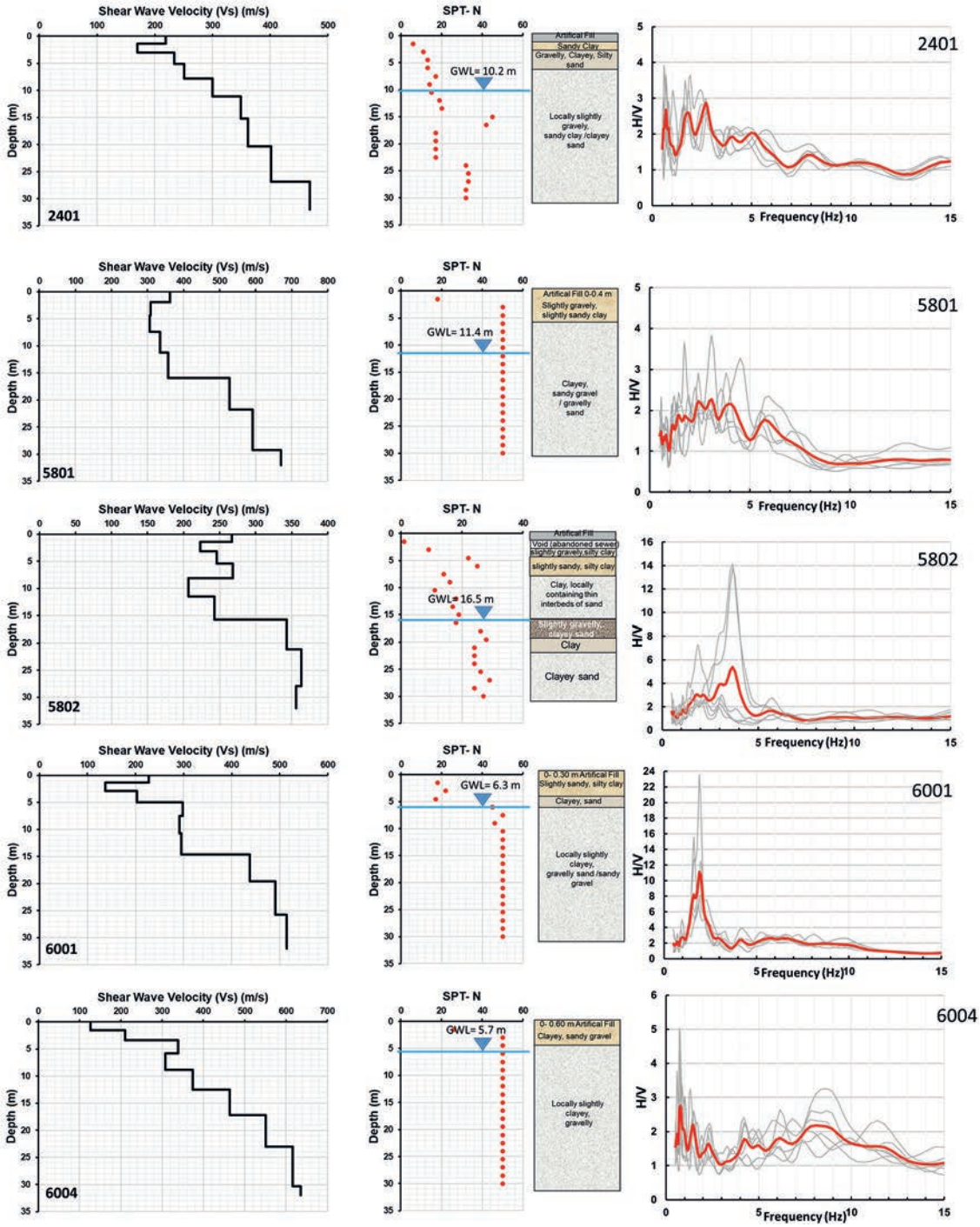

Fig. 8 - V_S-depth cross-sections, SPT-N values, borehole results and EHVs for the detailed stations (2401, 5801, 5802, 6001, 6004).

this station. In the bore log, at a depth of nearly 30 m, there are clayey and gravelly sand units. The peak amplitudes range between 0.8-3.0 Hz in the spectrum (Fig. 8). Station 5801 is located in the NE of Sivas. The V_S values range between 300 and 680 m/s from the surface to a depth of 30 m at this station. There is a relatively lower velocity layer between 3 and 15 m depth at this

Table 3 - Parameters of the selected earthquakes and the stations where they were recorded.

EQ no	Magnitude (Ml)	Date	Epicenter Coordinate	Depth (km)	Station name				
					2401	5801	5802	6001	6004
1	4.5	2008/06/04	39.63300N-39.02598E	18	*				
2	5.8	2010/03/08	38.77520N-40.02950E	5	*				
3	5.4	2011/09/22	39.65970N-38.67770E	7	*	*			
4	3.2	2013/11/20	39.40450N-40.13930E	10	*				
5	3.6	2014/05/03	39.70630N-38.85080E	7	*				
6	3.1	2014/06/25	39.90450N-39.50030E	8	*				
7	4.4	2012/01/14	40.06120N-38.34780E	14		*			
8	3.9	2013/04/28	40.04350N-38.23680E	6		*			
9	3.5	2013/07/24	40.29170N-37.93570E	15		*	*		
10	3.7	2013/11/22	39.64850N-38.21130E	7		*	*		
11	4.2	2014/09/20	39.16930N-38.72000E	8		*	*		
12	3.5	2013/05/27	40.05000N-38.72370E	17			*		
13	3.2	2013/09/12	39.95430N-37.55220E	14			*		
14	3.1	2013/10/23	39.87950N-38.80750E	11			*		
15	3.1	2011/05/14	40.29730N-36.42420E	8				*	
16	3.9	2013/02/27	40.29550N-36.45900E	13				*	
17	3.3	2013/05/01	40.62880N-36.80050E	14				*	*
18	3.7	2013/06/06	40.55600N-36.64330E	15				*	*
19	3.1	2013/06/28	40.47620N-36.98480E	16				*	
20	3.8	2013/08/04	40.53030N-36.95430E	14				*	*
21	3.6	2013/12/10	40.15680N-36.98820E	12				*	
22	3.5	2012/07/03	40.57200N-37.06580E	13					*
23	3.6	2013/01/02	40.58350N-37.09870E	2					*
24	3.3	2013/11/03	40.37400N-37.38330E	7					*

station. The SPT-N values at this station range between 18 and 50. The groundwater level for this station is at 11.4 m. In the bore log, there are clayey and gravelly sand units up to a depth of 30 m. The peak amplitudes are between 2.0-4.0 Hz in the spectra (Fig. 8). Station 5802 is located in the NE of Sivas. The V_S values range between 200 and 360 m/s from the surface to a depth of 30 m at this station. The relatively lower V_S layer of 8 to 16 m is noteworthy. The SPT-N values at this station are between 1 and 30. The groundwater level for this station is at 16.5 m. In the bore log, clayey and gravelly sand can be seen at a depth of nearly 30 m. The predominant amplitudes are between 3.0-5.0 Hz in the spectrum (Fig. 8). Examining station 6001, located on the Quaternary alluvium around Tokat, it is revealed that the V_S values vary between 150 and 510 m/s from the surface to a depth of 30 m. The SPT-N values at this station are between 18-50. The groundwater level for this station is at 6.3 m. In the bore log, there are clayey and gravelly sand up to a depth of nearly 30 m. The peak amplitudes are between 1.5-2.5 Hz in the spectra (Fig. 8). Examining

station 6004, located in the NE of Tokat, it can be seen that the V_S values vary between 110 and 620 m/s from the surface to a depth of 30 m. The SPT-N values at this station are between 24 and 50. The groundwater level for this station is at 5.7 m. It can be seen in the bore log that there are clayey and gravelly sand up to a depth of 30 m. The predominant amplitudes are between 0.5-2.0 Hz in the spectrum (Fig. 8).

7. Discussion and conclusion

This study presents the results of integrated geophysical and seismological investigations together with geotechnical studies in the northern part of the eastern Anatolian region (Turkey) with the aim of understanding local site effects for estimating seismic damage.

In this study, local soil effects were investigated using the EHV method for 30 stations. For data, six different earthquakes were used for each station. Examining the calculated EHV spectra it is revealed that there are not many changes in the spectra depending on the direction in general. Although scattering in amplification values were seen, amplification peak frequency values are often very similar. In stations 2902, 5808, and 5819, direction-dependent changes were observed in the calculated EHV spectra. Scattering at these stations is often seen at high frequencies. In addition, several peaks were obtained in the EHV spectra at some stations (2407, 2411, 2803, 5806, 5810, and 5812). This means that, in the case of soil structures with two or more strong impedance conditions, more than one peak can be obtained depending on the impedance differences. The largest of the multiple peaks seen in the EHV spectra obtained for these stations was chosen as the dominant frequency. These values were used as the predominant frequencies in mapping. Although the EHV spectra obtained at stations 2902, 5803, and 5813 appear to be a flat curve, amplification values above 2 are noteworthy.

The results can be summarised as follows. An amplification factor of approximately 10.5 was obtained for Tokat. The V_{S30} values are between 250-350 m/s in this region. The predominant period values are between 0.5 and 0.7 s. *Kg* values are greater than 20 in Tokat. The depth of the bedrock is between 30-40 m in this area. Amplification factors between 3.5 and 5.0 were obtained in the northern part of Tokat (Niksar, Erbaa). In this region, V_{s30} values are between 250-350 m/s, the predominant period values are between 0.3 and 0.8 s, *Kg* values are between 8 and 16, and the depth of the bedrock is between 20-50 m. The amplification factor is below 3 around Sivas. In this region, the V_{S30} values are between 650-750 m/s, the predominant period values are between 0.10 and 0.25 s, *Kg* values are less than 10, and the depth of the bedrock is between 10-20 m. The amplification factors were between 4 and 6 in the south-western part of Sivas (Şarkışla, Gemerek). In this region, the V_{s30} values are between 350-450 m/s, the predominant period values are between 0.3 and 0.5 s, *Kg* values are between 10 and 18, and the depth of the bedrock is between 10-30 m. The amplification factors range between 3.5 and 4.5 in the south-eastern part of Sivas (Kangal). In this region, the predominant period values are between 0.3 and 0.4 s, *Kg* values are between 5 and 10, and the depth of the bedrock is between 10-20 m. The amplification factors range between 2.5 and 3.0 in Giresun. In this region, the predominant period value is above 1 s, *Kg* values are less than 10 in, and the depth of the bedrock is approximately 100 m. The amplification factors range between 4.0 and 5.5 in Gümüşhane and the south-eastern part of Gümüşhane. In this region, the predominant period values are between 0.3 and 0.5 s, *Kg* values are between 5 and 10, and the

depth of the bedrock is between 10-30 m in this area. The V_{S30} values range between 450-550 m/s in Gümüşhane. The V_{S30} values range between 550-650 m/s in the southern part of Gümüşhane (Kelkit). The amplification factors range between 2.5 and 3.5 in the Erzincan basin. In this region, the predominant period values are between 0.4 and 0.6 s, *Kg* values are between 4 and 12, the depth of the bedrock is between 10-40 m, and the V_{S30} values are between 250-350 m/s. Amplification factors between 4.5 and 5.5 were obtained in western parts of Erzincan city (Akıncılar, Gölova, Refahiye). In this region, the predominant period values are between 0.2 and 0.5 s, *Kg* values are between 5 and 10, and the depth of the bedrock is between 10-30 m.

The predominant period map of soil obtained using the EHV method and earthquake data shows a very irregular distribution of values. This situation can be explained by the lateral heterogeneity of subsurface soil conditions in the study area. The predominant period is 0.05-1.20 s, which indicates that the area exhibits lower predominant periods and comprises less sediment thickness. Lower predominant period values (t_0 < 0.3 s) were detected in Sivas and the eastern parts of the city, composed of Miocene Limestone and Eocene carbonates and volcanics. It was noticed that Tokat and its surroundings, Giresun, and the Erzincan Basin all have high predominant period values (t_0 > 0.5 s). If the dominant period of the building and the soil predominant period values are close to each other, soil-structure resonance may occur. In this case, structures in the resonance are more damaged. The fundamental periods of N-story buildings can be approximately obtained using N/10 (s). Because the soil predominant period values in Tokat and its surroundings are between 0.5 and 0.7 s, resonance may occur in 5-to-7 storey buildings during an earthquake. In addition, because the soil predominant period values in the Erzincan Basin are between 0.4 and 0.6 s, resonance may occur in 4-to-6 storey buildings during an earthquake. 4-to-6 storey buildings in the Erzincan Basin and 10-12 storey buildings in Giresun and its surroundings also have this risk. In addition, the soil predominant period map should be considered to reduce the risk of resonance in building designs in new city plans.

V_S is a key parameter to characterise seismic site response modelling for earthquake-resistant design and to evaluate the dynamic behaviour of soil in the shallow subsurface. The V_{S30} values range from 250 to 750 m/s in the study area at 11 sites. Lower V_{S30} values were (250-350 m/s) obtained in the eastern part of Sivas (station 5802) on Miocene limestones, on clastics and evaporites in Tokat (station 6001) and the northern part of Tokat (station 6005), and in the Erzincan Basin (stations 2401 and 2407), located in alluvial units. V_S is directly related to lateral deformations of soil under earthquake loading. Deformations occurring during an earthquake exceed the elastic limit in these regions. Therefore, these regions may experience more damage than other areas during an earthquake. In these regions, bedrock depth at 30 m could not be reached according to V_{S30} values. For this reason, site-specific elastic spectra are recommended for earthquake-resistant design and new construction of buildings.

Bedrock depth also influences the amplification of the strong ground motion. The higher soil amplification values indicate that the amplitude of the earthquake waves will be increased by soil layers during an earthquake. Soil amplifications and predominant periods increase along with the thickness of the soil layers on bedrock. The amplification values in the study area vary between 2 and 11, while bedrock depth varies between 0 and 110 m. The deepest bedrock depth (80-110 m) was obtained in Giresun and the eastern part of Tokat. 2D or 3D soil-bedrock models should be established in regions where the soil thickness is more than 30 m for soil deformation analysis. In other words, seismic impedance must be determined from the bedrock in order to

calculate the earthquake effect on the surface within these regions. The sediment thickness is high in areas where predominant period values are high. Such soils have the property of increasing the magnitude and duration of earthquakes.

In this study, the *Kg* values, which are very important in hazard assessment, range from 1 to 30. According to *Kg* values, it can be said that Tokat and its surroundings and the south-western part of Sivas are weak zones. Sivas, the western part of Erzincan, Gümüşhane, and the south-eastern part of Gümüşhane have *Kg* values lower than 10, which indicates that those areas are less prone to seismic damage. The *Kg* index map can be used to estimate areas that could be damaged by future earthquakes. *Kg* mainly reflects ground strain during an earthquake. Therefore, it is necessary to make safe preparations for future earthquakes.

The water table in the study area is close to the surface, ranging from 5.7 to 16.5 m, and is especially shallow at stations 6001 and 6004. Since these areas have a risk of liquefaction during an earthquake, these areas should be examined in detail.

According to the results for the study area, the south-western part of Sivas, Tokat and its surroundings, Giresun and its surroundings, and Erzincan and its surroundings can be severely affected by strong ground motion. The predominant period, *Kg*, amplification, and bedrock maps of the study area can be used as a basis for planning future housing. As this study was carried out on a regional scale, it is recommended to increase the seismic networks and to apply geophysical, geological, and geotechnical studies in areas of high risk.

REFERENCES

Adib A., Afzal P. and Heydarzadeh K.; 2015: *Site effect classification based on microtremor data analysis using a concentration-area fractal model*. Nonlinear Processes Geophys., **22**, 53-63.

Arslan M., Tüysüz N., Korkmaz S. and Kurt H.; 1997: *Geochemistry and petrogenesis of the eastern Pontide volcanic rocks, northeast Turkey*. Chem. Erde, **57**, 157-187.

Babacan A.E. and Akın Ö.; 2018: *The investigation of soil-structure resonance of historical buildings using seismic refraction and ambient vibrations HVSR measurements: a case study from Trabzon in Turkey*. Acta Geophys., **66**, 1-21.

Barka A. and Gülen L.; 1989: *Complex evolution of the Erzincan Basin (eastern Turkey) and its pull-apart and continental escape origin*. J. Struct. Geol., **11**, 275-283.

Barka A., Akyüz H.S., Cohen H.A. and Watchorn F.; 2000: *Tectonic evolution of the Niksar and Tasova-Erbaa pull-apart basins, North Anatolian Fault Zone: their significance for the motion of the Anatolian block*. Tectonophys., **322**, 243-264.

Bektaş O., Yılmaz C., Tasli K., Akdağ K. and Özgür S.; 1995: *Cretaceous rifting of the eastern Pontides carbonate platform (NE Turkey): the formation of the carbonate breccias and turbidites as evidences of a drowned platform*. Geol., **57**, 233-244.

Beroya M.A.A., Aydin A., Tiglao R. and Lasal M.; 2009: *Use of microtremor in liquefaction hazard mapping*. Eng. Geol., **107**, 140-153.

Bonilla L.F., Steidl J.H., Lindley G.T., Tumarkin A.G. and Archuleta R.J.; 1997: *Site amplification in the San Ferdinando Valley, California: variability of site effect estimation using S-wave, coda, and H/V methods*. Bull. Seism. Soc. Am., **87**, 710-730.

Delgado J., Casado C.L., Lopez Giner J., Estevez A., Cuenca A. and Molina S.; 2000: *Microtremors as a geophysical exploration tool: applications and limitations*. J. Pure Appl. Geophys., **157**, 1445-1462.

Dinesh B.V., Nair G.J., Prasad A.G.V., Nakkeeran P.V. and Radhakrishna M.C.; 2010: *Estimation of sedimentary layer shear wave velocity using micro-tremor H/V ratio measurements for Bangalore city*. Soil Dyn. Earthquake Eng., **30**, 1377-1382.

Emre Ö., Duman T.Y., Özalp S., Elmaci H., Olgun Ş. and Şaroğlu F.; 2013: *Geological Map of Turkey at 1:500,000 scale*. General Directorate of Mineral Research and Exploration (MTA), Ankara, Turkey.

Gedikoğlu A., Pelin S. and Özsayar T.; 1979: *The main lines of geotectonic development of the east Pontids in Mesozoic age*. In: Proc., 1st Geological Congress of the Middle East, Ankara, Turkey, pp. 555-580.

Ibs-von Seth M. and Wohlenberg J.; 1999: *Microtremor measurements used to map thickness of soft sediments*. Bull. Seismol. Soc. Am., **89**, 250-259.

Konno K. and Ohmachi T.; 1998: *Ground-motion characteristics estimated from spectral ratio between horizontal and vertical components of microtremor*. Bull. Seismol. Soc. Am., **88**, 228-241.

Kyaw Z.L., Pramumijoyo S., Husein S., Fathani T.F. and Kiyono J.; 2014: *Investigation to the local site effects during earthquake induced ground deformation using microtremor observation in Yogyakarta, central Java-Indonesia*. In: Sassa K., Canuti P. and Yin Y. (eds), Landslide science for a safer geoenvironment, Springer, Cham, Switzerland, pp. 241-249.

Lachet C., Hatzfeld D., Bard P.-Y., Theodulidis N., Papaioannou C. and Savvaidis A.; 1996: *Site effects and microzonation in the city of Thessaloniki (Greece): comparison of different approaches*. Bull. Seismol. Soc. Am., **86**, 1692-1703.

Langston C.A.; 1977: *Corvallis, Oregon, crustal and upper mantle receiver structure from teleseismic P and S waves*. Bull. Seismol. Soc. Am., **67**, 713-724.

Lermo J.F. and Chavez-Garcia F.J.; 1993: *Site effect evaluation using spectral ratios with only one station*. Bull. Seismol. Soc. Am., **83**, 1574-1594.

Molnar S., Cassidy J.F., Castellaro S., Cornou C., Crow H., Hunter J.A., Matsushima S., Sanchez-Sesma F.J. and Yong A.; 2018: *Application of microtremor horizontal-to-vertical spectral ratio (MHVSR) analysis for site characterization: state of the art*. Surv. Geophys. **39**, 613-631.

MTA; 2002: *Geological map of Turkey at 1:500,000 scale*. General Directorate of Mineral Research and Exploration (MTA), Ankara, Turkey.

Nakamura Y.; 1997: *Seismic vulnerability indices for ground and structures using microtremor*. In: Proc., World Congress on Railway Research, Firenze, Italy, 1-7.

Nakamura Y.; 2000: *Clear identification of fundamental idea of Nakamura's technique and its applications*. In: Proc., 12th World Conference on Earthquake Engineering, Auckland, New Zealand, paper 2656.

Ozer C.; 2016: *Analysis of soil transfer function in Izmir Metropolitan Area, Turkey*. IOSR J. Appl. Geol. Geophys., **5**, 63-70, doi: 10.9790/0990-0501026370.

Ozer C.; 2019: *Investigation of the local soil effects of Erzurum and its surroundings using SSR and HVSR methods*. DEU J. Faculty Eng., J. Sci. Eng., **21**, 247-257, doi: 10.21205/deufmd.2019216124, in Turkish.

Pamuk E., Özdağ Ö.C., Tunçel A., Özyalın Ş. and Akgün M.; 2018: *Local site effects evaluation for Aliağa/İzmir using HVSR (Nakamura technique) and MASW methods*. Nat. Hazards, **90**, 887-899.

Parolai S.; 2012: *Investigation of site response in urban areas by using earthquake data and seismic noise*. In: Bormann P. (ed), New manual of seismological observatory practice 2 (NMSOP-2), Deutsches GeoForschungsZentrum GFZ, Potsdam, Germany, pp. 1-38, doi: 10.2312/GFZ.NMSOP-2_ch14.

Parolai S. and Richwalski S.M.; 2004: *The importance of converted waves in comparing H/V and RSM site responses*. Bull. Seismol. Soc. Am., **94,** 304-313.

Parolai S., Bormann P. and Milkereit C.; 2002: *New relationships between Vs, thickness of sediments, and resonance frequency calculated by the H/V ratio of seismic noise for the Cologne area (Germany)*. Bull. Seismol. Soc. Am., **92**, 2521-2527.

Şengör A.M.C., Tüysüz O., Imren C., Sakinç M., Eyidoğan H., Görür N., Le Pichon X. and Rangin C.; 2005: *The North Anatolian Fault: a new look*. Ann. Rev. Earth Planet. Sci., **33**, 37-112.

Sugianto N., Farid M. and Suryanto W.; 2016: *Local geology condition of Bengkulu city based on seismic vulnerability index (Kg)*. ARPN J. Eng. Appl. Sci., **11**, 4797-4803.

Tatar O., Akpinar Z., Gürsoy H., Piper J.D., Kocbulut F., Mesci B.L., Polat A. and Roberts A.P.; 2013: *Palaeomagnetic evidence for the neotectonic evolution of the Erzincan Basin, North Anatolian Fault Zone, Turkey*. J. Geodyn., **65**, 244-258.

Warnana D.D., Ria R.A.A. and Widya Utama W.; 2011: *Application of microtremor HVSR method for assessing site effect in residual soil slope*. Int. J. Basic Appl. Sci., **11**, 73-78.

Yalcinkaya E. and Alptekin O.; 2005a: *Contributions of basin-edge-induced surface waves to site effect in the Dinar basin, southwestern Turkey*. Pure Appl. Geophys., **162**, 931-950.

Yalcinkaya E. and Alptekin O.; 2005b: *Site effect and its relationship to the intensity and damage observed in the June 27, 1998 Adana-Ceyhan earthquake*. Pure Appl. Geophys., **162**, 913-930.

Yilmaz A. and Yilmaz H.; 2006: *Characteristic features and structural evolution of a post collisional basin: the Sivas Basin, central Anatolia, Turkey*. J. Asian Earth Sci., **27**, 164-176.

Corresponding author: Eren Pamuk
Department of Geophysical Research, MTA
(General Directorate of the Mineral Research & Exploration of Turkey)
Dumlupinar street, 06800 Ankara, Turkey
Phone: +90 312 2011000, e-mail: eren.pamuk@mta.gov.tr